BIOCHEMISTRY
including biophysical chemistry & molecular biology

ARTICLE

pubs.acs.org/biochemistry

Dynamic Ensemble View of the Conformational Landscape of HIV-1 TAR RNA and Allosteric Recognition

Jia Lu,[†] Beena M. Kadakkuzha,[†] Liang Zhao,[†] Martin Fan,[†] Xin Qi,[‡] and Tianbing Xia*[,†]

[†]Department of Molecular and Cell Biology, The University of Texas at Dallas, Richardson, Texas 75080, United States

[‡]Department of Chemistry and Medicinal Chemistry, The Scripps Research Institute, Scripps Florida, Jupiter, Florida 33458, United States

Supporting Information

ABSTRACT: RNA conformational dynamics and the resulting structural heterogeneity play an important role in RNA functions, e.g., recognition. Recognition of HIV-1 TAR RNA has been proposed to occur via a conformational capture mechanism. Here, using ultrafast time-resolved fluorescence spectroscopy, we have probed the complexity of the conformational landscape of HIV-1 TAR RNA and monitored the position-dependent changes in the landscape upon binding of a Tat protein-derived peptide and neomycin B. In the ligand-free state, the TAR RNA samples multiple families of conformations with various degrees of base stacking around the three-nucleotide bulge region. Some subpopulations partially resemble those ligand-bound states, but the coaxially stacked state is below the detection limit. When Tat or neomycin B binds, the bulge region as an ensemble undergoes a conformational transition in a position-dependent manner. Tat and neomycin B induce mutually exclusive changes in the TAR RNA underlying the mechanism of allosteric inhibition at an ensemble level with residue-specific details. Time-resolved anisotropy decay measurements revealed picosecond motions of bases in both ligand-free and ligand-bound states. Mutation of a base pair at the bulge−stem junction has differential effects on the conformational distributions of the bulge bases. A dynamic model of the ensemble view of the conformational landscape for HIV-1 TAR RNA is proposed, and the implication of the general mechanism of RNA recognition and its impact on RNA-based therapeutics are discussed.

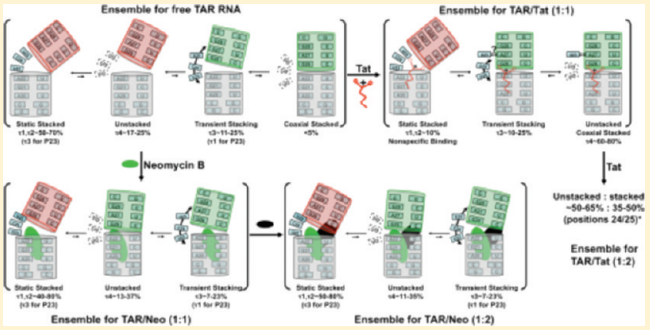

After decades of extensive investigation of structural biology, it is increasingly realized that motions of macromolecules are important for life processes. A complete description of biomolecular function requires in-depth understanding of the nature and functional role of conformational dynamics in addition to static high-resolution three-dimensional coordinates. It has been hypothesized that RNA ground state conformational dynamics can significantly enhance RNA's functional capacity compared to a static structure.[1,2] Some recent examples have shown that dynamic regions of RNAs are indeed often functionally important.[3−7] Different ranks of intricate RNA dynamics over a vast range of time scales, from femtoseconds to hours,[8] reflect RNA's elasticity and plasticity and have an impact on its recognition mechanism, e.g., conformational capture or induced fit mechanism.[2,9,10] Therefore, understanding the very rugged energy landscape of RNA structures is fundamentally important for elucidating the structure−dynamics−function relationship.[11]

The HIV-1 TAR RNA is an essential element of gene regulation located at the 5′-end of the viral transcript and is the binding site for the virally encoded Tat protein.[12,13] The HIV-1 TAR RNA features a stem−loop structure with a three-base bulge between two helical stems capped by a six-nucleotide apical loop (Figure 1A). High-resolution structural analyses showed that in the free RNA, the three bases of the bulge partially stack between the two stems,[14−18] causing a pronounced kink of up to ∼50° (Figure 1B)[19−22] or 25° if twisting motions are taken into account depending on how the two helical segments are viewed from each other,[23] but this bent structure apparently represents only an average structure. The RNA itself is very dynamic and samples a wide range of conformations with different degrees of base stacking around the bulge region.[16−18,24,25] The two relatively rigid helical regions undergo large amplitude correlated interhelical twisting and bending motions about the average bent structure.[5,18,20,23,24,26,27] The A22-U40 base pair, which is a confluence point for local and global dyamics, is not a canonical Watson−Crick pair and may be only partially formed.[5,16,18,23]

The bulge widens the RNA major groove.[16,28,29] When Tat binds, the three bases of the bulge are unstacked,[15] with U23 forming a base triple with the A27-U38 base pair based on NMR evidence[14,17,21,30,31] and molecular dynamics simulations.[24] In

Received: April 3, 2011
Revised: May 10, 2011
Published: May 10, 2011

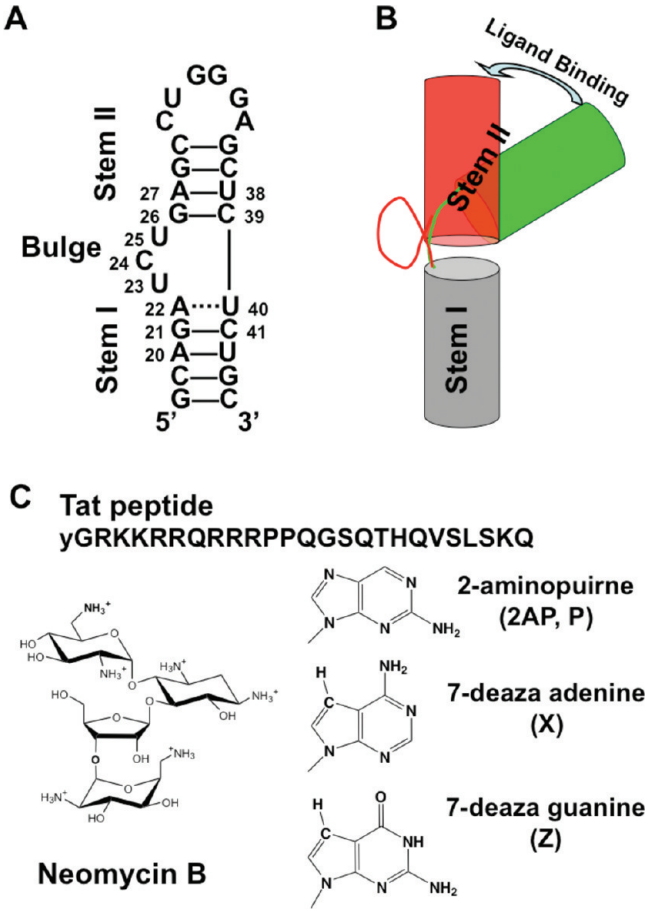

Figure 1. Structural representations of the HIV-1 TAR RNA and ligands. (A) Secondary structure of HIV-1 TAR RNA, with stems I and II, and the three-base bulge indicated. (B) Schematic model of ligand-induced interhelical domain motion. Stem I is represented by a gray cylinder, and stem II of the free RNA and stem II in complexes are represented by green and red cylinders, respectively. The curved arrow indicates the change in the bending angle between the two stems. (C) Sequence of the arginine-rich motif of HIV-1 Tat peptide and chemical structure of neomycin B and nucleobase analogues used in this study, 2-aminopurine (2AP or P), 7-deazaadenine (X), and 7-deazaguanine (Z).

addition, the two helices are brought into coaxial stacking, where the two base pairs, A22-U40 (now as a canonical pair) and G26-C39, flanking the bulge are directly stacked, leading to straightening of the helical segments (Figure 1B).[19] These conformational changes are key signatures of the structural transition of the HIV-1 TAR RNA upon formation of the complex. TAR−Tat interactions are mostly mediated by a single arginine residue within the arginine-rich motif of Tat (Figure 1C), and the role of this arginine[32] in the context of the basic region of the Tat protein can be largely captured by binding of a free amino acid arginine[14,19,33,34] or its analogue argininamide (ARG).[15,21,33] Other small molecules, including various antibiotics [e.g., neomycin B (Figure 1C)] and even cations, can also induce some of the features associated with the structural transition to different extents,[19,21,22,35−39] therefore partitioning the RNA into an equilibrium of free and ligand- or metal ion-bound states.

Dynamics of HIV-1 TAR RNA at the residue level, including picosecond to nanosecond fast motions and microsecond to millisecond slow motions, have been extensively probed by solution NMR[1] and EPR[25,40−43] methods. In particular, residual dipolar coupling[20−23,38,39] and spin relaxation measurements[5,44] have been very instrumental in resolving the multitude of motional modes, especially when coupled to the domain elongation approach[5,23,45] or in combination with molecular dynamics simulations.[18,46,47] It seems that the bulge in effect acts as a hinge for domain motions.[24] The free RNA samples local fluctuations on ∼30 ps time scales and rigid body domain reorientation between the two helical segments on ∼2 ns time scales.[5] Solid state deuterium NMR[48,49] fills the gap in the time scales that cannot be accessed by solution NMR and revealed significant nanosecond to microsecond motions within the bulge region, where U23 transiently unstacks from A22 on the microsecond time scale and also undergoes small amplitude twisting about the glycosidic bond on the ∼100 ps time scale, while U25 jumps between intrahelical and extrahelical states and also twists on a large amplitude scale over slow microsecond time scales. Binding of Tat peptide,[44] Mg^{2+},[38] Na^{+},[22] ARG,[5,21,44] and neomycin B[39] arrests interdomain motions and local fluctuations of the A22-U40 base pair, inducing coaxial stacking while promoting dynamics at looped out bases C24 and U25.

Particularly interesting with respect to this work, some of this early work suggested that a hierarchical network of local and collective motional modes on fast picosecond to nanosecond time scales is linked to TAR RNA's ability to adaptively change conformations upon binding by different ligands.[5] These conformations are within an ensemble including those similar to the ligand-bound forms that are distinct from each other.[5,18,20,23,27] Interestingly, these distinct conformations seem to fall along a narrow dynamic trajectory adapted by the RNA,[20,23,27] largely defined by topological constraints encoded by the two-way junction secondary structure architecture.[27] Binding of different ligands seems to stabilize distinct existing RNA conformations rather than inducing new ones, consistent with the concept of conformational selection or capture,[10,27,49] where tertiary interactions or ligand binding stabilizes one competent conformation by providing additional interactions. The similar time scales between global reorientation of the domains and the motions of the bases in the bulge seem to suggest that these motions may be correlated for ligand binding.[49]

Despite the broad range of experimental and computational approaches that are being used to probe motions across the RNA conformational landscape,[50] how fast motions in RNA impact its function is still poorly understood. Therefore, it is important to adequately characterize the full spectrum of RNA dynamics from ultrafast time scales to slow time scales. These characterizations require quantitative resolution of an ensemble of heterogeneous conformations resulting from the dynamics into individual subpopulations and the precise structural nature of each subpopulation in the free and complexed states. It is still difficult to resolve the heterogeneity of RNA structures quantitatively at atomic- or residue-specific levels because some of the conformational interconversions are too fast and some conformations are only transiently populated. The ability to capture and characterize the multiple alternative conformations, including minor populated states, can be as important as characterizing the predominant states, because oftentimes it is the minor population that is selectively stabilized during the recognition process via conformational capture.[51] It was envisioned that the combination of new NMR methods and complementary fluorescence techniques would provide an opportunity for probing dynamics over a wider

range of time scales.[52] Fluorescence spectroscopy with low time resolution may resolve some events of conformational transitions on a slower time scale and can detect only the subpopulation whose structure leads to slow fluorescence decay and would miss those subpopulations with fluorescence decay on distinct and potentially heterogeneous fast time scales and conformational dynamics that occur faster than the time resolution. This calls for new approaches capable of providing such valuable structural information with high spatial and temporal resolution. Here, we have used ultrafast dynamics-based approaches[6,11,51,53−57] to dissect the dynamic behaviors of HIV-1 TAR RNA. Results from these investigations are combined with findings from previous research using other powerful approaches, allowing us to quantitatively model the RNA structure as a dynamic ensemble and capture the changes upon engaging interactions to advance our understanding of the detailed mechanism of ligand binding-dependent allosteric recognition of this viral RNA.

EXPERIMENTAL PROCEDURES

Materials. All of the RNA constructs were purchased from Dharmacon (Lafayette, CO) and purified by polyacrylamide gel electrophoresis. RNA concentrations were calculated from UV absorbance measurements at 260 nm using extinction coefficients provided by Dharmacon. The oligos were dissolved in sodium phosphate buffer [20 mM sodium phosphate, 25 mM NaCl, and 0.1 mM EDTA (pH 6.8)] for all experiments and annealed by being heated to 95 °C for 1.5 min, followed by snap cooling on ice. Neomycin trisulfate salt hydrate (Neomycin B) was purchased from Sigma (catalog number N1876). The arginine-rich motif of Tat protein (Tat peptide) was synthesized and purified by the Protein Chemistry Technology Center at the University of Texas Southwestern Medical Center (Dallas, TX).

Steady State Fluorescence Spectroscopy. Steady state fluorescence titrations were performed on a Shimadzu spectrofluorophotometer (RF-5301PC) equipped with a temperature control module that maintains the sample temperature at 25 °C for all measurements, and the samples were constantly stirred during the collection of data. The excitation wavelength was 320 nm, and the emission wavelength was 370 nm. RNA concentrations were 200 nM to effectively measure two dissociation constants ranging from low nanomolar to low micromolar. Titration was conducted by adding 1−4 μL aliquots of Tat peptide or neomycin B solutions at a concentration of 5, 20, 40, or 180 μM into the RNA solutions. All measurements were taken in at least triplicate. Dissociation constants (K_d) were determined by fitting the binding isotherm using Dynafit.[58]

Isothermal Titration Calorimetry (ITC). All the ITC measurements were performed on a MicroCal iTC$_{200}$ microcalorimeter (Microcal, Inc.) as described previously.[51,57] Measurements were performed at 25 °C using 10 μM RNA and 500 μM neomycin B in the identical sodium phosphate buffer. Neomycin B ligand was titrated to the RNA in 25 injections of 0.5−2 μL aliquots with the reference power set at 6−7 μcal/s using an initial delay of 60 s with 120 s between injections and a 1000 rpm stirring speed. Data collected were fit to a model of two sets of binding sites using Origin 7.0 ITC (Microcal Software Inc.), and a χ^2 test was used to analyze the improvement over a single-site binding model. The two-site binding model improved the fit for all profiles (χ^2 values range from 10^3 to 10^4) compared to the one-site model (χ^2 values range from 10^4 to 10^5).

Femtosecond Time-Resolved Fluorescence Up-Conversion. The experimental setup and strategy for time-resolved fluorescence up-conversion spectroscopy have been published previously.[59] Briefly, femtosecond pulses (120 fs, 800 nm, 2.3 mJ) are generated from a Ti:sapphire laser system (Spectra Physics). The pulse is split equally into two beams, with one beam directed to pump an optical parametric amplifier (OPA) and the signal output quadrupled to generate the excitation pump pulse at 320 nm. The remainder of the fundamental 800 nm is used as the probe pulse. The emission from the sample cell is collected by a pair of parabolic focus mirrors and mixed with the probe pulse in a BBO crystal. The up-converted signal at 257 nm (up-converted from 380 nm) is detected with a photomultiplier after passing through a double-grating monochromator. All measurements were taken at 22 °C with an RNA concentration of 120 μM. For magic angle measurements, the pump beam polarization was set at 54.7° with respect to fluorescence polarization set by the BBO crystal. The femtosecond transients were collected up to 400 ps, and the final profile was the average of ∼200 transients that allowed us to analyze the data with uncertainty in the fitted parameters within 5%. The decay profiles were fit to a sum of multiple-exponential functions convoluted by a Gaussian instrument response function using the mathematical software Scientist as described previously, and statistical tests including χ^2 and F tests were used to determine the minimum model that can account for the decay profiles.[6,51,57,59]

Femtosecond Time-Resolved Fluorescence Anisotropy. Fluorescence transients with polarizations parallel and perpendicular to that of the excitation beam, $I_{||}(t)$ and $I_{\perp}(t)$, were separately collected and then calibrated as described previously.[6,51,56,57,59] To account for the possible fluctuation of the excitation power between the two separate independent measurements, we measured the fluorescence intensities for a solution of free 2AP base at two time delay points, one in the negative time regime (e.g., −10 ps) and the other after a long delay time (e.g., 400 ps), following each transient acquisition of the RNA constructs. The fluorescence intensity of 2AP at −10 ps was used for background correction. After a time delay of 400 ps, the anisotropy of free 2AP base should have completely decayed to zero, and an identical intensity of 2AP fluorescence should be observed between parallel and perpendicular polarizations. The differences in the intensities between these two time delays of −10 and 400 ps for parallel polarization and perpendicular polarization were used to calibrate the two polarization transients of RNA constructs. The femtosecond time-resolved anisotropy, $r(t)$, was then fit with a multiple-exponential function.

RESULTS

Design and Biophysical Characterization of the TAR RNA Constructs. Specific considerations for designing RNA constructs that contain fluorescent probes for ultrafast time-resolved fluorescence spectroscopy have been discussed in depth elsewhere.[59] We obtained a series of 27-nucleotide HIV-1 TAR RNA constructs with 2-aminopurine [2AP, denoted as P (Figure 1C)] incorporated at various positions, including A20 (P20), A22 (P22), U23 (P23), C24 (P24), U25 (P25), and A27 (P27). A second set of constructs feature the A22-U40 to G22-C40 mutation (WT-GC, P23-GC, P24-GC, and P25-GC). Labeling the RNA at these different positions allows us to probe the different regions of the RNA, including the two stems and the bulge, to analyze how the conformational dynamics and the associated

Table 1. Dissociation Constants (K_d) of Tat and Neomycin B Binding to HIV-1 TAR RNA Constructs

	Tat binding		neomycin B binding			
	steady state fluorescence		steady state fluorescence		ITC	
construct[a]	K_{d1} (nM)	K_{d2} (μM)	K_{d1} (nM)	K_{d2} (μM)	K_{d1} (nM)	K_{d2} (μM)
WT					32 ± 5	2.6 ± 0.6
P20			(7)[b]	0.5 ± 0.2	7 ± 3	4.6 ± 0.3
P20Z21					9 ± 5	2.3 ± 0.6
P22			11 ± 5	0.8 ± 0.1	4 ± 2	4.5 ± 0.3
P22Z21			14 ± 5	0.9 ± 0.08	12 ± 6	1.6 ± 0.4
P22Z26			48 ± 6	6.4 ± 1.3	~1[c]	2.3 ± 1
P23			22 ± 5	5.8 ± 0.6	14 ± 1	5.2 ± 0.3
P23X22			17 ± 4	1.9 ± 0.6		
P24	60 ± 10	~1[d]	4 ± 1	0.7 ± 0.06	22 ± 6	3.6 ± 0.3
P24X22			4 ± 2	0.2 ± 0.07		
P24Z26			5 ± 1	0.4 ± 0.03	34 ± 8	5.6 ± 0.8
P25	6 ± 2	~0.1[d]	13 ± 2	2.5 ± 0.4	8 ± 1	2.4 ± 0.7
P25Z26			14 ± 2	0.3 ± 0.04		
P27			280 ± 53	3.1 ± 1.3	7 ± 1	3.3 ± 0.1
WT-GC					29 ± 8	3.1 ± 0.3
P23-GC			6 ± 3	5.1 ± 1.6	10 ± 6	3.2 ± 0.1
P24-GC	7 ± 3	~1[d]	9 ± 3	4 ± 1	15 ± 7	4 ± 1
P25-GC	2 ± 1	0.1 ± 0.01	2 ± 3	0.2 ± 0.04	~10[c]	3.7 ± 0.6

[a] Constructs are denoted by the positions labeled with 2AP (P) and 7-deazaguanine (Z) or 7-deazaadenine (X). Uncertainties in parameters were estimated from multiple measurements. [b] Because of the extremely small amplitude of the overall fluorescence change, K_{d1} for P20 was fixed on the basis of ITC measurement (7 nM). [c] Values are only estimates determined with Origin. [d] Values are only estimates because of the small amplitudes of signal changes for the second binding event.

changes in the dynamics upon ligand binding depend on the structural context. HIV-1 TAR RNA with C24 or U25 mutated to purine retains the wild-type affinity for Tat,[28,60] and constructs with 2AP incorporated at these positions have proven to be useful in previous steady state fluorescence experiments.[61] Additional constructs with either a guanine base replaced with 7-deazaguanine (Z) or an adenine base replaced with 7-deazaadenine (X) (Figure 1C) have also been obtained for the purpose of making specific assignments of decay components. These modified bases quench 2AP fluorescence on ~1 and ~4 ps time scales, respectively, which are unique rates that are faster than those observed for their natural base counterparts.[6,59,62] We recently demonstrated that incorporation of such modified bases at a unique site can provide unambiguous site-specific information regarding the nature of direct base stacking interactions in RNA motifs and thus facilitated assignments of specific interactions.[6,51,55−57]

Binding of Tat peptide or other ligands to these TAR RNA constructs is an appropriate functional assay for validating these constructs. Our own steady state fluorescence titration performed on constructs P24 and P25 showed that these RNAs can form 1:1 and 1:2 complexes with the Tat peptide (Table 1 and Figrue S1 of the Supporting Information), with the binding affinities (K_{d1} = 6−60 nM; K_{d2} = 0.1−1 μM) being very similar to the previously reported values for the wild-type RNA or with 2AP labeled at these two positions,[12,61] including the direction of fluorescence changes. Steady state fluorescence (Figure S1 of the Supporting Information) and isothermal calorimetry (ITC) measurements (Figure 2 and Figure S2 of the Supporting Information) upon binding of neomycin B to these designed constructs also showed two sets of binding sites (note the kink in the ITC profiles that indicates two binding events), first with low nanomolar and second with low micromolar affinities (Table 1), similar to those reported earlier for unlabeled wild-type (WT)[63] or 2AP-labeled constructs.[61] These biophysical characterizations validated the use of such constructs for probing HIV-1 TAR RNA conformational dynamics. The steady state fluorescence intensity of the free RNAs and the changes in the intensity upon ligand binding hinted at the nature of the local structure of the RNA and its changes at the probe site but necessarily reflect only the population-averaged structural information. The resolution of subpopulations can be achieved via time-resolved spectroscopy with sufficient time resolution to distinguish the distinct fluorescence decay dynamics signatures of 2AP incorporated in the RNA, where the multitude of conformations is reflected by the multiexponential nature of the decay dynamics profiles.

HIV-1 TAR RNA Features Position-Dependent Conformational Heterogeneity in the Free State. The first major questions we wish to address are the level of complexity of the conformational landscape of the free RNA and the extent to which the various bound states are dynamically sampled in the free RNA.[1,20,23,27] We have collected the ultrafast decays for all of the RNA constructs in the free state in the absence of divalent ions (Figure 3A). These and other decay profiles (Figure S3 of the Supporting Information) were fit to multiexponential functions, and careful statistical analysis, including the χ^2 test and F test,[59] showed that three to four decay components are needed to adequately account for the decay dynamics (Figure S4 of the Supporting Information). These multiphasic decay profiles suggest that the RNA indeed samples various degrees of heterogeneous

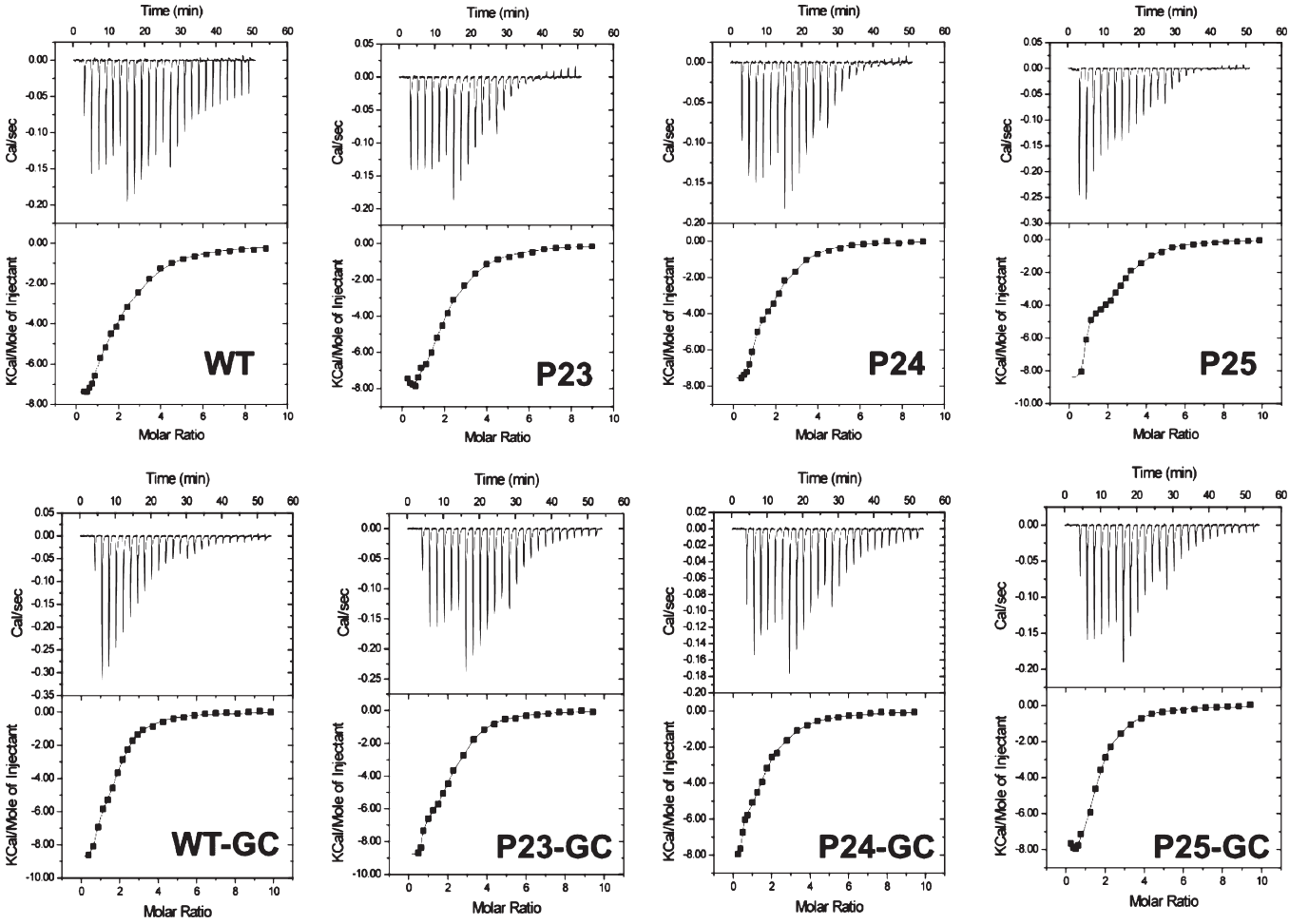

Figure 2. Isothermal titration calorimetry measurements of dissociation constants (K_d) for neomycin B binding to HIV-1 TAR RNA constructs of WT, P23, P24, P25, WT-GC, P23-GC, P24-GC, and P25-GC. All transitions were fit to a model of two sets of binding sites, which is apparent from the shapes of these transitions, with the first K_d values in the low nanomolar range and the second K_d values in the low micromolar range.

conformations depending on the region. Table 2 lists all the decay dynamics parameters in detail.

P20 and P22 within lower stem I and P27 within upper stem II have more pronounced fast decay dynamics (τ_1 = 1.6−3 ps, τ_2 = 7.8−12 ps, and τ_3 = 77−153 ps, with a total amplitude of 94−95%), consistent with these bases being mostly stacked with neighboring GC base pairs within helical regions, either statically (τ_1) or dynamically with small amplitude base flipping motions (τ_2 and τ_3).[6,51,56] Small populations of the unstacked state (τ_4 = 11.3 ns, ∼5−6%) due to breathing are still detected. In a comparison of the profiles of P22 and P22Z21 (Figure 3B), the presence of a 1.1 ps component of 72% for P22Z21 uniquely defines the P22/Z21 direct static base stacking[6,51,55,56] but also suggests that this A22-U40 pair is not fully formed as a static structure because it is close to the dynamic bulge region. Previous NMR experiments also suggested that the A22-U40 pair is only transiently formed in the absence of ligand.[15−17,21] The decay profiles for P22 and P22Z26 are very similar, particularly in the lack of an ∼1 ps component for P22Z26 that would be a unique indicator for direct stacking between A22-U40 and Z26-C39 base pairs that is seen in the structures of arginine- or ARG-bound complexes[14,15] to produce such a signal. This suggests that the fully coaxially stacked population in the free RNA is very small (<5%).

For the bulge region, the decay profiles are very heterogeneous. The decay profile for P24 indicated that there are at least four different families of conformations for this base in terms of stacking interactions, with similar populuations, and none represents a dominant population. Base 24 may stack with base 23 or 25 of the neighboring bulge pyrimidine bases (τ_1 and τ_2),[64] or other bases in certain conformations where base 23, base 25, or both are flipped out. Base 24 also has a larger totally unstacked population (25%) compared to other stem positions. For construct P25, the fastest component (τ_1 = 1.9 ps) represents the stacking of P25 with G26, which accounts for approximately half (53%) of the total population. Apparently, this base 25/base 26-stacked subpopulation is in dynamic equilibrium with other dynamically stacked conformations (τ_2 = 9.6 ps, and τ_3 = 92 ps) and with a totally unstacked state represented by the 11.3 ns component with a 17% amplitude. Construct P25Z26 has a 1.4 ps decay component corroborating the stacking interaction between bases 25 and 26 in a subpopulation. Base P25 behaves somewhat like that of a 5′-dangling purine on a GC or ZC base pair,[56] suggesting that the intrinsic property of a dangling end base may play a major role in the population distribution within the bulge region in the free RNA state.

These findings suggest that the bulge bases flip between stacked and unstacked states, and the stacked states feature

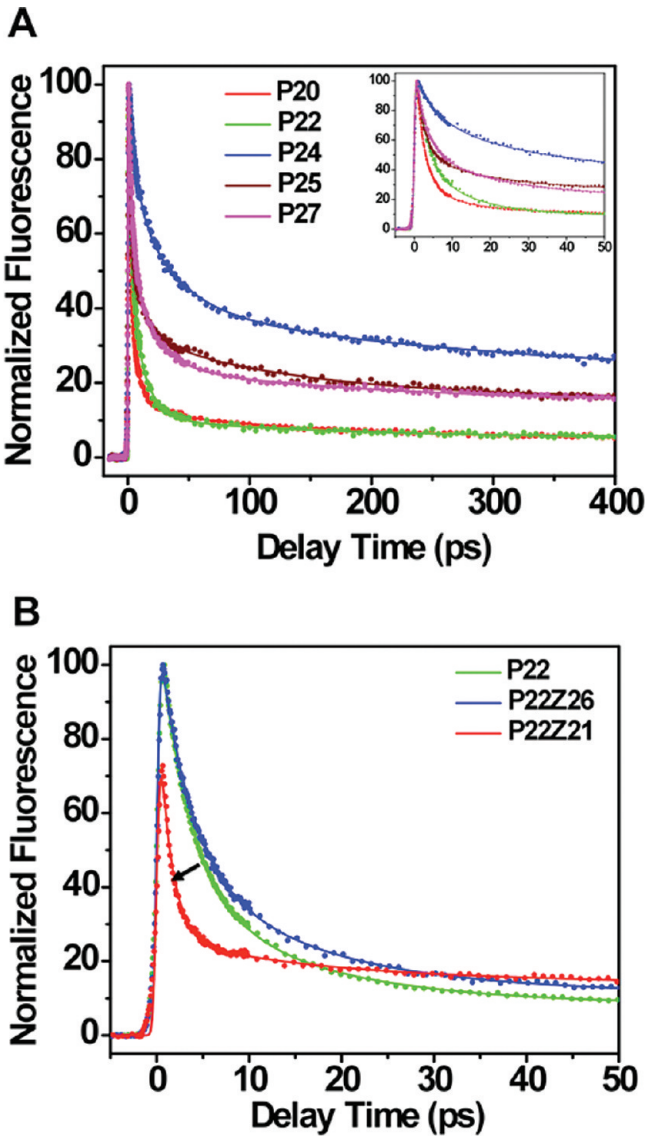

Figure 3. Femtosecond time-resolved fluorescence decay profiles at the magic angle for HIV-1 TAR RNA constructs in the ligand-free state. (A) Fluorescence decays for constructs P20 (red), P22 (green), P24 (blue), P25 (brown), and P27 (magenta). The inset shows a shorter time window. (B) Comparison of decay profiles for constructs P22 (green) with P22Z21 (red) and P22Z26 (blue). The arrow indicates the change in the dynamics time scale of the fastest component from P22 (2.9 ps) to P22Z21 (1.1 ps). The decrease in the initial intensity for P22Z21 is due to the presence of the ultrafast dynamics (1.1 ps), where there is already significant decay within the finite pulse width.

heterogeneous populations, consistent with previous reports based on NMR evidence that the bases transiently loop out of the helix in the ligand-free state.[16−18,24,25] Such looping out of the bulge bases is necessary for ligand binding. Our data provide precise and quantitative information about the distribution of the subpopulations.

Distinct Ligand Binding-Induced Changes in the Conformational Landscape. The next major question is how the different ligands alter the population distributions observed for the free RNA.[27] With information about the various signatures of heterogeneous stacking interactions in different regions of the RNA in the ligand-free state, we then examined the effects of binding of different ligands, including Tat peptide and neomycin B (Figure 1C), on the observed landscape, to map out the ligand-dependent structural transitions associated with formation of a specific complex.[44] We anticipate that the TAR complexes also feature a certain degree of dynamics, either more restricted or enhanced compared to that of the free RNA depending on the locations of the bases that are probed.

Changes in the steady state fluorescence intensity of TAR constructs P24 and P25 were observed upon Tat peptide binding, where an initial increase in fluorescence intensity, 3.3- and 6.4-fold, respectively, was followed by a smaller (15 and 19%, respectively) decrease (Figure S1 of the Supporting Information). This is consistent with two binding events, i.e., formation of a specific 1:1 complex and formation of a non-specific complex.[12] Neomycin B binding induces similar changes for P24, where formation of a 1:1 complex increases the fluorescence (although the amplitude is smaller, 1.9-fold, compared to the Tat-induced increase) and formation of 1:2 complex deceases it slightly (26%). For neomycin B binding of P25, however, an only 10% fluorescence decrease versus that of free RNA was observed for the first binding event followed by another 33% decrease, different from the binding of Tat peptide. Similar observations have previously been made on constructs equivalent to our P24 and P25.[61] In principle, steady state fluorescence changes should be reflected in corresponding changes in time-resolved decays because the steady state intensity is the integration of the time-resolved profile over time, where only the slow nanosecond components make a significant contribution to the overall steady state quantum yield. These changes in decay profiles can be captured, providing important information for the mechanism of conformational transitions.

Figure 4 shows changes in ultrafast dynamics decay profiles upon binding of Tat peptide and neomycin B for constructs P24 and P25, and neomycin B for P23. For P24, upon formation of a 1:1 complex with Tat peptide, significant changes in the decay profile were observed (Figure 4A), where the amplitude of the nanosecond (τ_4) component is significantly increased from 25% in the free state to 79% in the complex (Table 2). Similarly, this is observed for P25 (Figure 4B), where Tat binding induces a large increase in the nanosecond components from 17 to 61%. This indicates that both bases 24 and 25 sample more totally unstacked population in the complex with Tat peptide, consistent with these bases flipping out in the complex in the NMR structure.[15] Note the presence of smaller but detectable amplitudes of ultrafast decay components ($\tau_1-\tau_3$, total amplitudes of 21 and 39% for P24 and P25, respectively) even in the 1:1 complexes, which revealed that the complex structure is still heterogeneous, and these bases at least transiently interact with the rest of the RNA and undergo charge transfer reactions in minor subpopulations. In comparison, Tat binding does not significantly alter the decay profiles for P20 and P22 in the lower stem (Figure S3 of the Supporting Information) and only slightly stabilizes the base-paired structures by increasing the stacked population. Because 2AP at either base 23 or base 27 is expected to disrupt the formation of the U23:A27-U38 base triple, their decay profiles for Tat complexes are not discussed here. Because of precipitation when the peptide:RNA ratio is greater than 1:1 at the high concentrations required for ultrafast dynamics experiments, the decay dynamics for the RNA:peptide complex at a >1:1 stochiometry were not determined.

Binding of neomycin B in the minor groove of HIV-1 TAR RNA is known to allosterically inhibit TAR−Tat interactions by

Table 2. Parameters of Femtosecond Time-Resolved Fluorescence Quenching Dynamics[a]

construct	τ_1 (ps)	A_1 (%)	τ_2 (ps)	A_2 (%)	τ_3 (ps)	A_3 (%)	τ_4 (ns)[b]	A_4 (%)
P20 (free)	1.9	67	7.8	21	118	7	11.3	5
P20/Tat (1:1)	2.0	73	9	20	242	5	11.3	2
P20/Neo (1:1)	2.2	74	28	18			11.3	8
P20/Neo (1:2)	1.6	58	6.8	29	98	8	11.3	5
P20Z21 (free)	0.8	50	8.2	19	122	18	11.3	13
P20Z21/Tat (1:1)	1.0	46	6	22	96	20	11.3	12
P20Z21/Neo (1:1)	0.8	55	7.6	18	112	16	11.3	11
P20Z21/Neo (1:2)	0.8	58	7.1	18	99	15	11.3	9
P22 (free)	2.9	60	12.2	31	153	4	11.3	5
P22/Tat (1:1)	2	69	9	24	75	4	11.3	3
P22/Neo (1:1)	2.3	52	9.8	37	100	6	11.3	5
P22/Neo (1:2)	2.5	54	10.8	36	113	6	11.3	4
P22Z21 (free)	1.1	72	10.9	12	150	7	11.3	9
P22Z21/Tat (1:1)	1.2	80	16	9	385	9	11.3	2
P22Z21/Neo (1:1)	1.1	72	6.4	12	116	8	11.3	8
P22Z21/Neo (1:2)	0.9	73	5.2	14	86	7	11.3	6
P22Z26 (free)	3.4	57	13.5	30	117	6	11.3	7
P22Z26/Neo (1:1)	2.5	44	11.9	33	132	11	11.3	12
P22Z26/Neo (1:2)	2.6	47	12.6	34	140	9	11.3	10
P23 (free)	17.8	25			148	49	11.3	26
P23/Neo (1:1)	12.4	23			111	42	11.3	35
P23/Neo (1:2)	13	23			106	53	11.3	24
P23X22 (free)	6.3	30	43	22	327	32	11.3	16
P23X22/Neo (1:1)	5.1	24	27	20	197	26	11.3	30
P23X22/Neo (1:2)	6	30	31	26	295	20	11.3	25
P24 (free)	3.3	23	21	35	170	17	11.3	25
P24/Tat (1:1)	4.3	5	14	6	172	10	11.3	79
P24/Neo (1:1)	3.8	25	24	20	231	18	11.3	37
P24/Neo (1:2)	3.5	28	21	22	168	15	11.3	35
P24X22 (free)	5.6	32	24	36	152	16	11.3	16
P24X22/Neo (1:1)	5.6	33	27	28	185	16	11.3	23
P24X22/Neo (1:2)	6.2	37	33	26	213	16	11.3	21
P24Z26 (free)	6.6	29	30	28	180	20	11.3	23
P24Z26/Neo (1:1)	5.8	23	25	17	179	22	11.3	38
P24Z26/Neo (1:2)	4.4	21	20	19	180	23	11.3	37
P25 (free)	1.9	53	9.6	19	92	11	11.3	17
P25/Tat (1:1)	7.4	13			175	26	11.3	61
P25/Neo (1:1)	2	52	8.4	28	74	7	11.3	13
P25/Neo (1:2)	2.4	56	10.7	26	88	7	11.3	11
P25Z26 (free)	1.4	30	14	18	135	26	11.3	26
P25Z26/Neo (1:1)	1.2	30	11	18	126	24	11.3	28
P25Z26/Neo (1:2)	1.1	35	10.6	20	112	23	11.3	22
P27 (free)	1.6	76	8.1	15	77	3	11.3	6
P27/Tat (1:1)	2.1	66	10	16	84	8	11.3	10
P27/Neo (1:1)	1.7	72	13	17			11.3	11
P27/Neo (1:2)	1.4	55	6.9	23	46	9	11.3	13
P23-GC (free)	4.2	25	19	40	141	18	11.3	17
P23-GC/Neo (1:1)	4.2	21	20	34	163	22	11.3	23
P23-GC/Neo (1:2)	4.3	23	20	35	140	19	11.3	23
P24-GC (free)	7.4	26	43	22	543	22	11.3	30
P24-GC/Tat (1:1)			9.7	16	134	14	11.3	70
P24-GC/Neo (1:1)			10.0	31	106	23	11.3	46
P24-GC/Neo (1:2)			9.0	37	102	22	11.3	41
P25-GC (free)	4.0	26	16	21	145	28	11.3	25

Table 2. Continued

construct	τ_1 (ps)	A_1 (%)	τ_2 (ps)	A_2 (%)	τ_3 (ps)	A_3 (%)	τ_4 (ns)[b]	A_4 (%)
P25-GC/Tat (1:1)			19	22	105	40	11.3	38
P25-GC/Neo (1:1)	7.5	33			95	32	11.3	35
P25-GC/Neo (1:2)	5.6	32	39	29	335	18	11.3	21

[a] τ_i and A_i are the decay lifetimes and pre-exponential amplitudes, respectively, for the ith exponential decay component. Estimated errors are ~5% based on two to three repeat measurements and previously published results. [b] τ_4 was fixed at 11.3 ns because of the short time window (up to 400 ps) of the femtosecond experiments.

inducing different structural changes in the RNA.[36,61,63,65] Figure 4 also shows the changes in the decay dynamics induced by neomycin B binding. Neomycin B causes much smaller increases in the nanosecond component for P24 for a 1:1 complex and a slight decrease upon formation of the 1:2 complex (Figure 4A). For P25, neomycin B binding slightly decreases the magnitude of the nanosecond component for both 1:1 and 1:2 complexes (Figure 4B). These results indicated different patterns of base stacking between the two positions, and both are different from changes induced by Tat binding. Here, with the ability to resolve precisely the different base stacking patterns at the residue level, we can begin to analyze the structural mechanism of such allosteric competition. Obviously, the two different ligands, Tat and neomycin B, induce mutually incompatible changes in the HIV-1 TAR RNA structure, at least in the bulge region. In comparison, neomycin B binding changed little of the overall dynamic profiles for positions in the lower stem (P20 and P22) or upper stem (P27) (Figure S3 of the Supporting Information).

Tat peptide does not bind the P23 construct with comparable affinity. Neomycin B, however, does bind the P23 construct with affinities [on the basis of ITC and steady state fluorescence titraion, K_{d1} = 14−22 nM and K_{d2} = 5.2−5.8 μM (Table 1)] similar to those of WT RNA and other constructs. This provides an opportunity to probe the conformational dynamics and heterogeneity of base 23 upon neomycin B binding. Figure 4C compares the fluorescence decay dynamics for free P23 and complexes with neomycin B. In the free state, P23 decay features three components. τ_1 (~18 ps) is on a similar time scale of quenching by a cytosine or uracil base,[64] likely due to stacking with neighboring C24 or U25 if C24 looped out to allow direct stacking between 23 and 25, while τ_3 (148 ps), which represents approximately half of the population, is due to stacking with an adenine base,[57,66] most likely A22. The presence of higher amplitudes of faster decay components in P23X22 is consistent with this assignment. The τ_4 component represents the totally unstacked population (26%) that is similar to those for bases 24 and 25. Upon formation of a 1:1 complex with neomycin B, there is an increase in the totally unstacked population (35%), while upon formation of the 1:2 complex, this population decreases (24%), indicating a similar degree of stacking compared to that of free RNA.

The evolution of decay dynamics profiles upon formation of complexes with Tat or neomycin B at positions P23, P24, and P25 is all quantitatively consistent with the steady state fluorescence titration profiles (Figure S1 of the Supporting Information). The steady state fluorescence titration profiles upon ligand binding can reveal significant structural information as demonstrated previously.[61] The ultrafast dynamics probing, however, can provide additional crucial structural information, particularly the population-resolved data that allow one to capture the structures and changes in structures from an ensemble point of view.

Directly Probing Time Scales of Dynamic Motions. Anisotropy measurements provide mobility information, including the time scales and amplitudes of probe base motions within the RNAs. Figure 5 shows the femtosecond time-resolved anisotropy decay profiles for P23, P24, and P25 in the free state and in complexes with either Tat or neomycin B. The parameters are listed in Table 3. The ~10 ns component (τ_3) in the anisotropy decays represents an estimate of time scales of the tumbling motion of the entire RNA or complexes, consistent with the size of the systems.[5] The presence of subnanosecond base motions for P23, P24, and P25 in the free state and in complexes with Tat or neomycin B indicated that these bases can undergo multiple modes of fast motions on picosecond to nanosecond time scales and therefore remain dynamic on picosecond time scales in all states, including the free and ligand-bound states. Motion on a time scale of tens of picoseconds (τ_1) is typical of rotation of the base about the glycosidic bond, and motion on a time scale of hundreds of picoseconds (τ_2) is likely local stacking−unstacking conformational sampling.[6] The relatively small amplitude values for these fast motions compared to the possible maximum value of 0.4 suggested that these motions are hindered, not freely rotating motions, which is typical for a nucleobase covalently attached to a nucleic acid backbone. These motions presumably allow the bases to sample different stacked and unstacked states that are separated by low barriers (less than a few kilocalories per mole). These picosecond to nanosecond motions also often contribute to the apparent time scales of the magic angle measurements via conformationally gated charge transfer[67] and therefore aid the interpretation of the intermediate time scale dynamics in the magic angle experiments.

Differential Effects of Base Pair Mutation at the Bulge−Stem Junction on Bulge Base Dynamics. Recently, it was demonstrated that the dynamics of free TAR RNA can be tuned to effect ligand binding.[68] For example, changing the noncanonical A22-U40 base pair that flanks the triple bulge to a more stable GC pair promoted in the free RNA those interactions and dynamics observed in the ARG-bound state by improving the stacking interactions with the G26-C39 pair. The interhelical motions are reduced with a nearly coaxially stacked conformation (12° bend angle). These changes led to a higher affinity of ARG for the mutant RNA. Consequently, ARG binding to the mutant RNA induced only minor further conformational changes. On the other hand, binding of neomycin B induces different changes compared to those observed in WT TAR RNA.[36] In other words, the conformational ensemble of TAR RNA[27] is now more preorganized toward the ARG-bound state, and this can be tested by the femtosecond dynamics approach.

We obtained HIV-1 TAR RNA constructs with the A22-U40 to G22-C40 mutation without 2AP (WT-GC) and with 2AP at positions 23 (P23-GC), 24 (P24-GC), and 25 (P25-GC) to

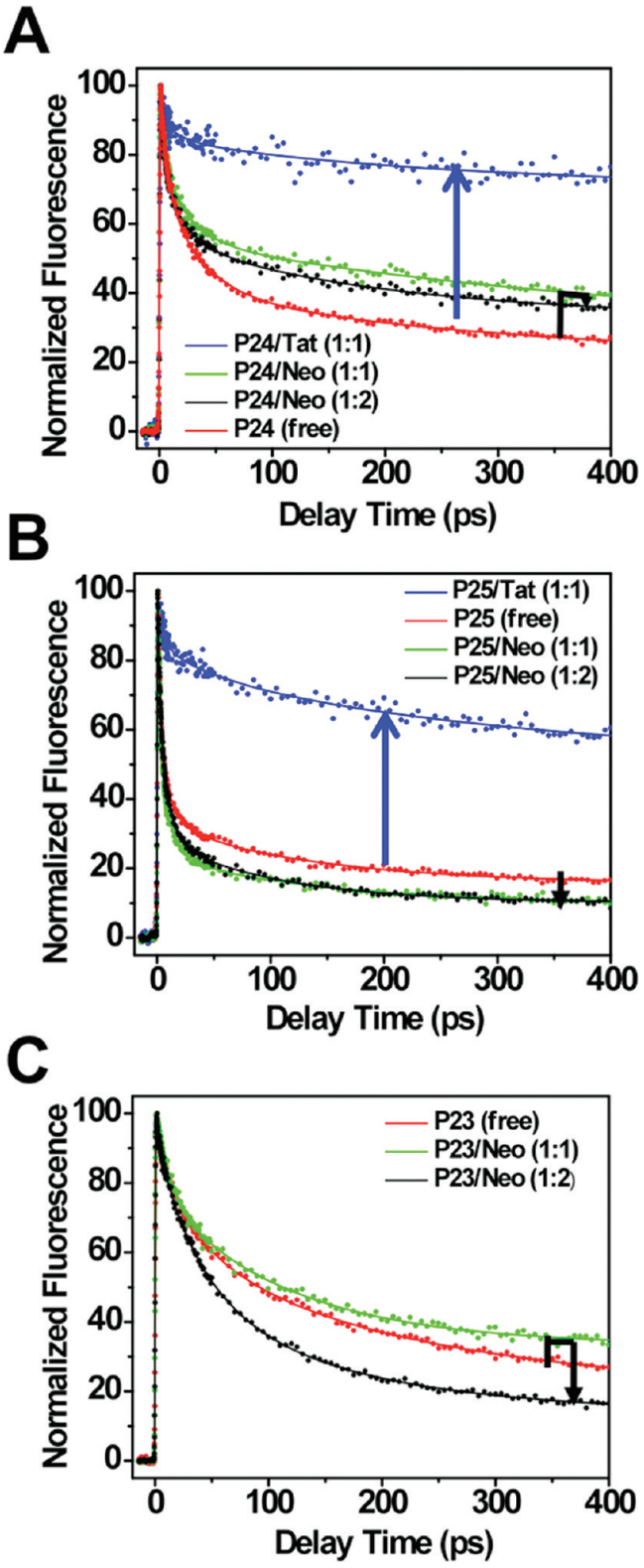

Figure 4. Comparisons of magic angle decay dynamics of free RNA and complexes with Tat or neomycin B: (A) decay profiles of P24, (B) decay profiles of P25, and (C) decay profiles of P23, for the ligand-free state (red) and the complexes with Tat (1:1, blue) or neomycin B at 1:1 (green) and 1:2 (black) ratios. Arrows indicate the direction of changes in the profile between the free TAR RNA and TAR−Tat (blue) or TAR−Neo complexes (black).

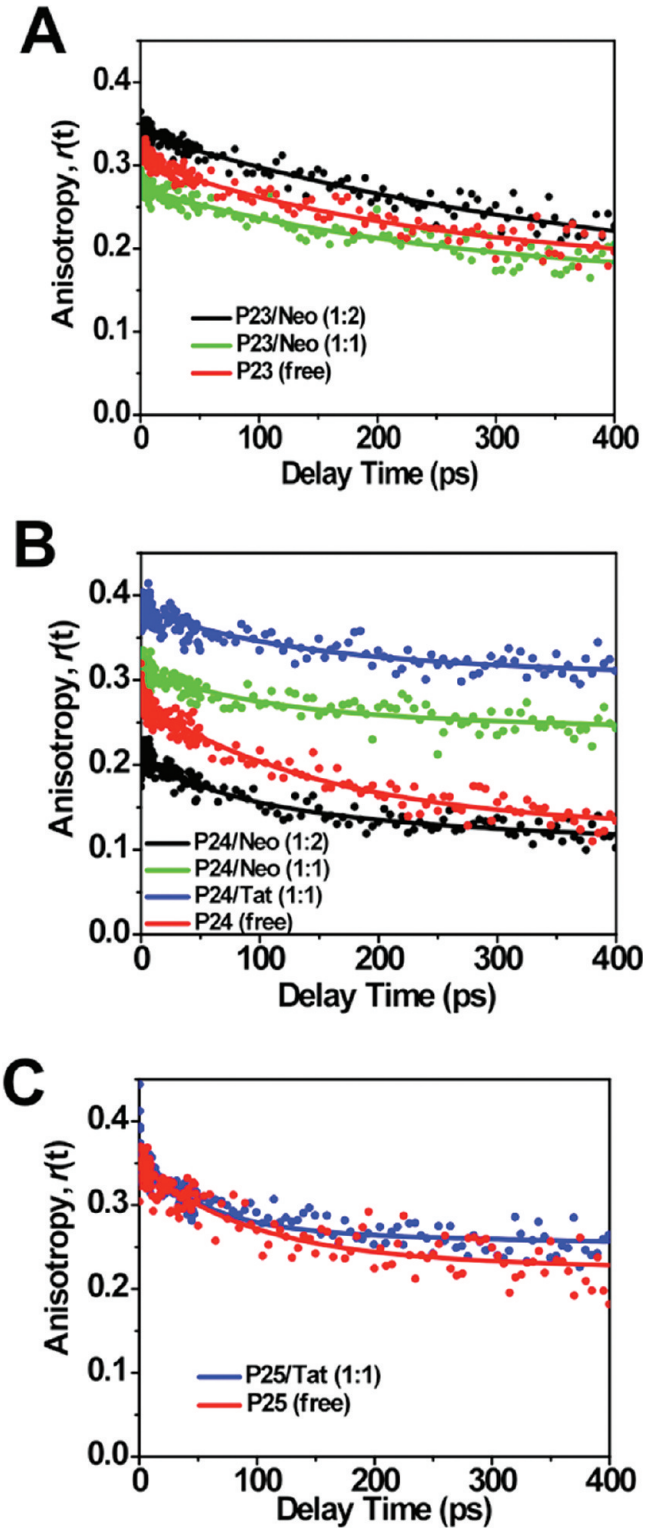

Figure 5. Femtosecond time-resolved fluorescence anisotropy decay dynamics for (A) P23, (B) P24, and (C) P25, in the ligand-free state (red) and in complexes with Tat (1:1, blue) or neomycin B at 1:1 (green) and 1:2 (black) ratios.

assess the shift in the conformational ensemble caused by this mutation. The decay profiles indicate that both P24-GC (Figure 6A) and P25-GC (Figure 6C) have larger unstacked populations in the free state than P24 and P25, respectively. This

dx.doi.org/10.1021/bi200495d |*Biochemistry* 2011, 50, 5042–5057

Table 3. Femtosecond Time-Resolved Anisotropy Decay Parameters[a]

construct	τ_1 (ps)	r_1	τ_2 (ps)	r_2	τ_3 (ns)	r_3	r_0[b]
P23 (free)	14	0.018	281	0.127	~10	0.175	0.320
P23/Neo (1:1)	24	0.008	281	0.105	~10	0.164	0.277
P23/Neo (1:2)	6	0.008	391	0.174	~10	0.165	0.347
P24 (free)			153	0.14	~10	0.13	0.27
P24/Tat (1:1)			117	0.06	~10	0.32	0.38
P24/Neo (1:1)			101	0.056	~10	0.257	0.313
P24/Neo (1:2)	59	0.044	231	0.055	~10	0.113	0.212
P25 (free)			92	0.11	~10	0.24	0.35
P25/Tat (1:1)			56	0.08	~10	0.27	0.35
P24-GC (free)			99	0.12	~10	0.22	0.34
P24-GC/Tat (1:1)			99	0.08	~10	0.21	0.29
P25-GC (free)			144	0.12	~10	0.16	0.28
P25-GC/Tat (1:1)			118	0.08	~10	0.18	0.26

[a] Anisotropy decay profiles are fit to two or three exponential terms (τ_1–τ_3). τ_3 should be considered as an estimate of decay on the nanosecond time scale, because of the limited experimental time window. Estimated errors in parameters are ~10%. [b] The fundamental anisotropy at time zero (r_0) is calculated as $r_0 = r_1 + r_2 + r_3$.

suggests that the mutation shifts the population toward the bound state that features larger looped out populations at these positions. This shift is not complete, and the presence of significant stacked states and heterogeneity is still apparent. For P23, a 4.2 ps component with a 25% population indicates its direct stacking with the G22 base (Figure S5 of the Supporting Information). The totally unstacked population, however, is reduced compared to that of P23 without the mutation, opposite to the effects of mutation on bases 24 and 25.

Tat binding to P24-GC still induces significant changes in the decay profile compared to the Tat-bound decay profile for P24. For P25-GC, however, Tat binding does not induce significant changes compared to that of the free P25-GC profile. It appears that for base P25, the A22-U40 to G22-C40 mutation has largely locked base 25 in a conformation preorganized for Tat binding, but distinct from that of the Tat-bound form for P25. The conformational heterogeneity at position 25, consequently, is not significantly altered. Time-resolved anisotropy decay measurements indicated that P24-GC and P25-GC are dynamic on ~100 ps time scales in both the free state and the Tat-bound state.

We then investigated whether or how neomycin B binding alters the ensemble of the mutant RNA in a manner different from that of WT. Neomycin B binding to P23-GC (Figure S5 of the Supporting Information) and P24-GC (Figure 6B) induces a small increase in the unstacked population followed by a small decrease, similar to the effects of neomycin B on P23 and P24 without the mutation. For P25-GC, however, neomycin binding induced a different response (Figure 6D); instead of a continuous decrease in the unstacked population, the binding first caused an increase followed by a decrease. All these changes in the time-resolved decay dynamics profiles are consistent with the corresponding steady state titration (Figure S1 of the Supporting Information), in terms of the difference in the fluorescence intensity of the free RNA with or without the mutation, and the changes in the intensities upon binding of Tat or neomycin B.

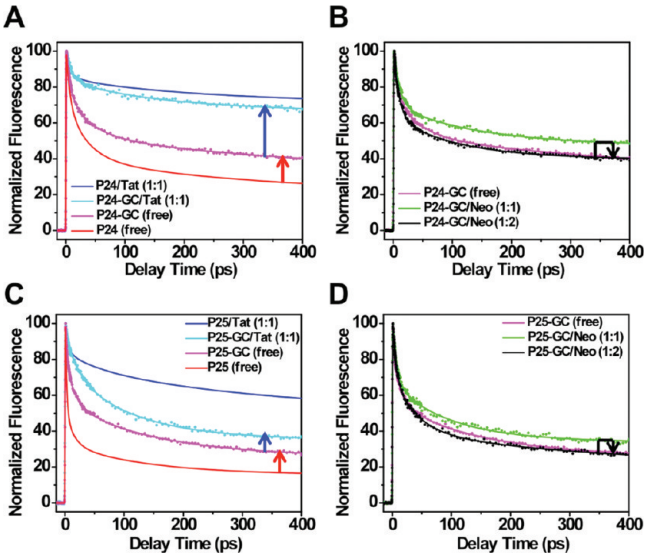

Figure 6. Effects of A22-U40 to G22-C40 mutations on the femtosecond time-resolved fluorescence decays for HIV-1 TAR RNA. Comparison of decay profiles between (A) P24 (red) and P24-GC (magenta) in the free state and in complexes with Tat P24/Tat (blue) and P24-GC/Tat (cyan), (B) P24-GC in the free state (red) and P24-GC/Neo complexes at 1:1 (green) and 1:2 (black) ratios, (C) P25 (red) and P25-GC (magenta) in the free state and in complexes with Tat P25/Tat (blue) and P25-GC/Tat (cyan), and (D) P25-GC in the free state (magenta) and P25-GC/Neo complexes at 1:1 (green) and 1:2 (black) ratios. Arrows indicate the changes in the decay profiles in the ligand-free states caused by the mutation (red) and induced by Tat binding to the mutated RNA constructs (blue). Black arrows indicate the changes induced upon neomycin B binding to the mutated RNAs.

DISCUSSION

Different RNA conformations within an ensemble may provide different local environments for the probe 2AP causing its fluorescence to decay due to charge transfer on distinct time scales that depend on the details of the structures and specific interactions involved. Therefore, the heterogeneous nature of the RNA structures renders the overall decay profile multiphasic in the picosecond to nanosecond time regime, reflecting multiple conformational states that coexist at equilibrium, if the interconversion of the conformations is slow within the experimental time window. Ultrafast dynamics probing allows one to capture conformational dynamics that occur on ultrafast time scales, extending the range of dynamics that can be probed into this regime to capture the elasticity of RNA conformations. More importantly, snapshots of multiple structures (plasticity) that undergo slower dynamic exchange and their intrinsic flexibility can be captured quantitatively to better define the ensemble and shape of the conformational landscape, producing unprecedented levels of detail on the intrinsic motions and heterogeneity of RNAs. Changes, if any, in the dynamics upon ligand binding can be monitored to provide insights into the detailed molecular mechanism of recognition of dynamic RNA structures.

Ensemble View of the Conformational Landscape. Taking together the data presented here, as well as existing high-resolution structures and dynamics information available in the literature, we propose a preliminary ensemble model for the dynamic conformational landscape of HIV-1 TAR RNA and its complexes with Tat and neomycin B (Figure 7).

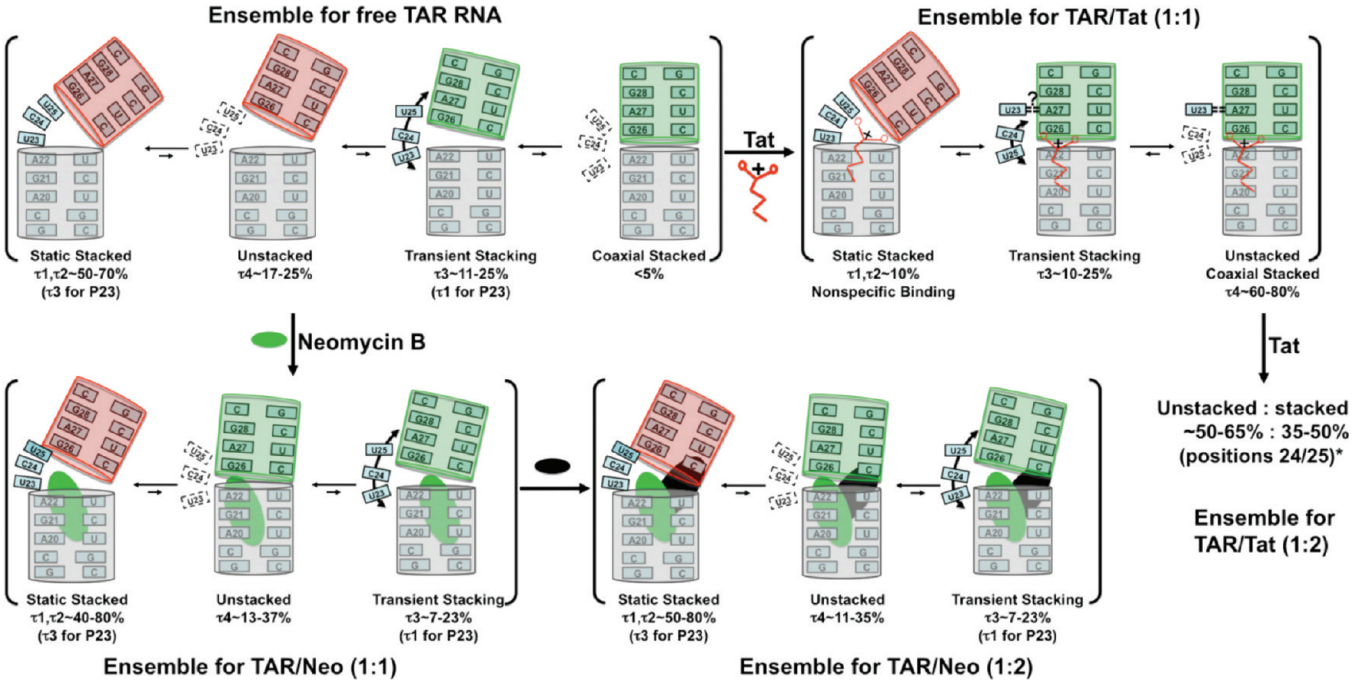

Figure 7. Dynamic ensemble structural model for HIV-1 TAR RNA and its complexes with Tat and neomycin. The two helical regions, stem I and stem II, are considered as rigid bodies (cylinder), and for the sake of clarity, the opening of base pairs (e.g., A22-U40) is not explicitly included. Red and green portions of upper stem II denote large and small helical angles with lower stem I, respectively. Dashed boxes for bases 23−25 indicate that their conformations are not uniquely determined. For the Tat complex, an arginine residue (red) is shown to represent the critical interactions between Tat peptide and TAR RNA (front side of RNA indicates major groove). The U23:A27-U38 base triple is included, but a question mark is shown to indicate the possibility that it may not form in the minor population. The curved double arrows indicate undefined stacking interactions with other bases. For neomycin B complexes, the binding pocket for the first neomycin B binding site (green) is well-defined (back side of RNA indicates minor groove), but the second binding site (black) has not been identified.

NMR and other evidence has shown that the HIV-1 TAR RNA samples a number of conformations with a dominant population that features stacking of all three bulge bases and therefore a large average interhelical angle of up to 25−50°.[19−21,23] The motions can be modeled as isotropic interhelical fluctuations within a cone with a radius angle of ~46°.[20] Such fluctuations would allow the RNA to populate tertiary conformations with interhelical angles between 0° and 90°, potentially including the coaxially aligned conformation (0°) as a minor population.[20] Our ultrafast dynamics probing revealed that indeed the RNA in the ligand-free state samples multiple families of conformations with different base stacking patterns around the bulge region (Figure 7). There is a major subpopulation (50−70%) in which all three bulge bases stack continuously on one strand causing a significant bend between the two helical stems. This structure is characterized by fluorescence decay dynamics τ_1 and τ_2 for bases P24 and P25 and τ_3 for P23. The tendency for these bases to partially stack on the stem is in part consistent with their intrinsic behavior as an unpaired nucleotide next to a flanking base pair.[56]

There is a minor subpopulation (17−25%) in which all three bases flip out without any base stacking interaction, characterized by the τ_4 component for each base. In another minor subpopulation (11−25%), these three bases may flip out but transiently stack with each other, and this is characterized by a decay component on a time scale of hundreds of picoseconds (τ_3 for P24 and P25) or tens of picoseconds (τ_1 for P23). Such time scales of decay lifetimes often indicate in part conformational gating in charge transfer reactions,[6,51,67] consistent with the observations of similar time scales of base motion from anisotropy decay data (Table 3). The two minor subpopulations would feature bending angles smaller than that for the major subpopulation. Apparently, the relatively nonspecific nature of base stacking interactions contributes to the ruggedness of the free RNA energy landscape. Base stacking and unstacking dynamics allow RNAs to sample multiple conformations of different stacking patterns that are separated by energetic barriers of various heights. Although NMR probing has suggested that the interhelical motions on microsecond to millisecond time scales may allow the TAR RNA to access the coaxially stacked conformation corresponding to the Tat-bound state,[20] our data showed that such a state has relatively small populations (<5%) viewed on the subnanosecond time scale.

Binding of Tat in the major groove induces significant changes in the dynamics profiles of the bulge bases and, therefore, the population distributions. Tat stabilizes a conformation that features coaxial stacking, and this conformation becomes a dominant population (60−80%) characterized by the τ_4 components of the bulge bases. However, this specific Tat-bound form is not the only population in the complex, and it is in equilibrium with minor populations in which the bulge bases may interact with other bases as revealed by the presence of ultrafast decay components. One of the minor populations promotes charge transfer of 2AP that is consistent with the continuous stacking of all three bulge bases, and we propose this represents nonspecific binding of Tat. We also note that the affinity of Tat peptide for the P25Z26 construct, where N7 of G26 is changed to a CH group, is siginificantly compromised, consistent with the fact that N7 of G26 is involved in a critical hydrogen bonding

dx.doi.org/10.1021/bi200495d |*Biochemistry* 2011, 50, 5042–5057

interaction,[14,15] and disruption of this single hydrogen bond is sufficient to abolish Tat binding. The TAR−Tat complex at a >1:1 ratio has not been adequately characterized structurally. Because of the precipitation problem with formation of the TAR−Tat complex at a stoichiometry of >1:1, dynamics experiments were not performed for higher-order RNA−peptide complexes. On the basis of steady state fluorescence measurements (Figure S1 of the Supporting Information), one can estimate that upon binding of a second Tat (most likely nonspecifically), the overall distributions of subpopulations shift slightly to favor more stacked states.

Neomycin B has been suggested to bind in the minor groove of the lower stem below the trinucleotide bulge based on footprinting and mutational studies[63] and NMR,[36] although MD simulation also suggested the possibility of major groove binding.[69] Circular dichroism spectroscopy,[63,65] NMR spectroscopy,[36] and steady state fluorescence evidence[61] showed that neomycin B binding induces changes in the TAR RNA structure distinct from those induced by Tat; e.g., neomycin B binding reduces the volume of the major groove where Tat binds[36] and consequently allosterically inhibits Tat binding.[36,61,63] The detailed mechanism of allosteric inhibition, however, was not clear.

Like those for the Tat complex, our dynamics data also suggested the heterogeneous nature of the neomycin B complex. When one or two neomycin B molecules bind, the major population (40−80 or 50−80%) features all three-bulge bases statically stacked with the two stems. This population is in equilibrium with at least two minor populations in which the bulge bases are flipped out. Such population distributions are consistent with the previous findings that neomycin B is known to bind a more bent (30°) TAR conformation on average.[27,36] However, observation of a nuclear Overhauser effect between A22 and G26 also indicated direct base stacking in the TAR−Neo complex that would lead to straightening of the helix. The subpopulation of the complex that features such interfacial coaxial stacking and unstacking of bulge bases is included in the ensemble. The coexistence of multiple conformations is presumably responsible for the line broadening and low NMR signals from the neomycin B ligand in the complex that preclude the complete assignments of resonances to individual protons.[36] The NMR study could not precisely define the locations of the bulge bases, presumably because of the multiple interconverting conformations of the bulge region.

Note that Tat binding and neomycin B binding induce differential changes, either qualitatively or quantitatively, in the dynamic decay profiles of HIV-1 TAR RNA; therefore, the directions of changes in the conformational ensembles of the Tat complex and neomycin B complex are mutually exclusive. This provides details about the mechanism of the nature of the allosteric inhibition of Tat binding by neomycin B.[36,61,63]

These population data can be directly used in a partition function analysis[51,57] to calculate the free energy difference between different states that range mostly within 1 kcal/mol at 22 °C with the population of the highest occupancy representing the ground state for each base. The model presented in Figure 7 should be considered a minimal model, as each subpopulation may still represent a family of closely related conformations that have not been uniquely resolved at all base positions because they may produce a similar decay dynamics profile with a probe at a certain position.

Biased Ensemble by Mutation at the Junction. Mutation of the A22-U40 base pair flanking the bulge region to a more stable G22-C40 pair noticeably affects the conformational equilibrium of the free RNA states, shifting bases 24 and 25 toward ARG-bound (unstacked) states to some extent[68] but far from completely locking them into the ARG-bound state. The effect on base 23 is the opposite. More interestingly, while Tat binding induces a similar significant conformational transition for base 24 for the mutated RNA, base 25 appears to be mostly locked in a different Tat-bound conformation by the mutation compared to that of the WT RNA. Neomycin B binding also produces different changes at base 25 compared to WT. Therefore, the base pair mutation at the junction of the bulge and stem I influences the most changes at the adjacent and most distant position from the mutation in the bulge, consistent with the fact that bases 23 and 25 are more critical than base 24, which serves as a linker.[12,60]

Base Motion on Picosecond Time Scales. The observed fluorescence decay dynamics measured at the magic angle reflect only the electronic interactions involving the probe and do not directly represent the RNA conformational motions per se. Femtosecond time-resolved fluorescence anisotropy measurements provide useful information about the actual time scales and amplitudes of dynamic motions of the probe.

NMR probing showed that the free RNA samples local fluctuations on picosecond to nanosecond time scales.[5,48,49] Anisotropy decay dynamics also revealed that there is a range of picosecond time scales over which conformational transitions can occur (Table 3). Motions on such picosecond to nanosecond time scales represent segmental or internal motion of certain amplitudes for the probe within the RNA structural contexts,[6,51,56,57,59] leading to heterogeneous nature of the structure and the multiphasic decay profiles of the magic angle experiments, providing kinetic information to define the barrier of the energy landscape. What is not clear from these data alone is whether the flipping-out motions of these bulge bases are concerted. Upon formation of the complex, the bulge bases remain dynamic on picosecond time scales. This information can complement slower nanosecond to millisecond dynamics information from other approaches.

Ultrafast Dynamics as a Complementary Approach. NMR probing has been the driving force in elucidating the conformational dynamics of HIV-1 TAR RNA. Our findings for the ensemble of subpopulations and the dynamic time scales form interesting and meaningful comparisons to those from NMR and other probing techniques. Each subpopulation detected here, however, may not directly correspond to a single conformation sampled by the RNA as revealed by NMR; instead, it is the heterogeneous nature at each base position that is captured by ultrafast dynamics. Such a dynamic picture at each base position reflects all the conformations collectively, including those that have been detected or still missed by all the techniques. The significance of our findings is that minor or alternative populations were detected and should be considered as an integral part of the ensemble picture. The fluorescence anisotropy decay data provide dynamics information about the base that can complement those for the comparable time scales by NMR or EPR. One of the limitations of the fluorescence approach is that it is sensitive to only base stacking interactions. For other interactions, e.g., hydrogen bonding, and their heterogeneous nature, NMR continues to be the technique of choice. In addition, computational approaches will be more meaningful with all these experimental constraints guiding and validating the simulation efforts.

Implications for the General Mechanism of RNA Recognition. Recent work suggested that the dynamic sampling of active and inactive conformations is built in protein structures through natural evolution, and substrate binding or post-translational modifications may act to shift a preexisting equilibrium.[70,71] What about RNAs? Plenty of evidence suggested that HIV-1 TAR RNA recognition is achieved via conformational capture.[2,5,18,20,23,27] In a conformational capture process, the ligand-bound form preexists within a conformational ensemble and can be detected at least by a certain technique. This subpopulation, oftentimes a minor population in free RNA, is stabilized by a ligand binding event that provides additional interactions, thereby shifting the conformational equilibrium toward the bound state. Such a mechanism has also been implicated, including evidence from ultrafast time-resolved fluorescence spectroscopy from this lab, in other RNA systems, e.g., theophylline-binding aptamer[51] and purine-sensing riboswitches.[72] Whether conformational capture or induced fit[9,10] versus conformational rearrangement is the main underlying mechanism operating in RNA recognition remains to be investigated in more systems.

The ultrafast dynamics probing of HIV-1 TAR RNA recogition suggested that bases 24 and 25 sample the bulged-out conformations with detectable populations. Such bulged-out states are requisite for forming the ligand-bound state, but the coaxially stacked state asscociated with the specific ligand binding, however, has a very small population (Figure 7) below the detection limit of ultrafast fluorescence spectroscopy. In other words, a combined conformational capture−induced fit mechanism must operate in such a system, where the conformations of the "preexisting" subpopulations in TAR RNA that were "captured" by various ligands may only partially resemble but are not identical to the true ligand-specific bound states, because certain interactions cannot be fulfilled in the absence of the ligands, particularly those directly involving the ligand moiety itself[14,15] as in the theophylline aptamer,[51] or if there is issue of entry of the ligand into a deeply buried pocket such as in the case of purine-sensing riboswitches.[72] Therefore, at least locally induced fit has to occur. A separate issue is how much of the population of the preexisting structure is necessary for one to consider that the conformational capture mechanism dominates the recognition process, which also relates to the sensitivity of a particular technique for detecting minor or even trace populations.

Therefore, there would be no conformational capture mechanism in a strict sense, and some degree of conformational rearrangements or induced changes at least locally if not globally is always necessary for specific recognition of a dynamic structure. In addition, as shown for the theophylline aptamer, an RNA structure may be mostly preorganized in one region but need to reorganize significantly in another region via capturing a preexisting local structure feature.[51] The partitioning of conformational capture and induced fit will certainly be position-dependent. Understanding how such partitioning depends on the structural context of RNAs poses a major challenge in RNA biophysics, and a combined approach using modern techniques, including NMR, EPR, time-resolved spectroscopy, single-molecule techniques, and molecular dynamics simulations, may continue to shed new light on the formulation of a new paradigm of RNA conformational dynamics.

Biomedical Significance of the Findings. Understanding the detailed recognition mechanism is an important issue as RNA has been increasingly recognized as a valid target for molecular therapeutic intervention. Recent efforts directed toward developing agents targeting RNA-based diseases, e.g., myotonic dystrophy type 1 that features long CUG repeats in mRNA, have seen some success.[73,74] In targeting RNA, specificity is much more challenging to achieve than affinity alone, and rules are actively being decoded.[75] The ultimate success of these efforts depends critically on a deep understanding of the impacts of conformational dynamics and structural heterogeneity on adaptive ligand recognition.[10,76] The dynamic nature of RNAs renders the structure-based ligand design a challenging task, because the ruggedness of the conformational landscape of the free RNA plays a very significant role. A recent study showed that a benzimidazole derivative compound binds a conformationally flexible structure within the internal ribosomal entry site (IRES) of the hepatitis C virus (HCV) and captures one of the specific structures of the ensemble, thereby locking the IRES in an inactive form.[77] Therefore, the challenge of targeting dynamic RNA structure can present itself as a unique opportunity if the conformational dynamics can be better understood.

In the past three decades since HIV was isolated, the AIDS pandemic remains one of the most devastating diseases in human history. Agents that can disrupt the function of HIV-1 TAR RNA may significantly interfere with viral gene transcription, representing a promising antiviral strategy. The findings reported here and previously allow one to incorporate dynamic information into the rational design of ligands to recognize the intrinsically dynamic TAR RNA, greatly facilitating structure-based rational designs of novel antiviral compounds.[78−80] In particular, a more complete picture of the structural ensemble of the target TAR RNA can suggest alternative structures, though present in only small populations or transiently, may contain more unique features than the dominant structures and, therefore, are valuable targets. Designing drugs against the more unique minor structure, thereby locking the target in the alternative conformations, may provide a viable pathway to achieving high specificity and high potency. Information about the intrinsic plasticity and elasticity of the targeted microstate therefore can be extremely useful for drug design. This will open up exciting opportunities for computer-aided modeling and screening of drug leads. The work reported here and future findings promise to contribute to such foundations.

■ ASSOCIATED CONTENT

Supporting Information. Steady state fluorescence titration and ITC measurements of Tat and neomycin B binding to HIV-1 TAR RNA constructs and femtosecond time-resolved fluorescence decay profiles and representative residual plots. This material is available free of charge via the Internet at http://pubs.acs.org.

■ AUTHOR INFORMATION

Corresponding Author

*E-mail: tianbing.xia@utdallas.edu. Phone: (972) 883-6328. Fax: (972) 883-2409.

Funding Sources

This work was partially supported by the THECB Norman Hackerman Advance Research Program (009741-0004-2006 and 009741-0015-2007) and the Robert A. Welch Foundation (AT-1645).

■ ABBREVIATIONS

TAR, transactivation response; Tat, transactivator of transcription; ARG, argininamide; Neo, neomycin B; 2AP, 2-aminopurine; Z, 7-deazaguanine; X, 7-deazaadenine; ITC, isothermal calorimetry; fwhm, full width at half-maximum; OPA, optical parametric amplifier; CT, charge transfer.

■ REFERENCES

(1) Al-Hashimi, H. M. (2005) Dynamics-based amplification of RNA function and its characterization by using NMR spectroscopy. *ChemBioChem 6*, 1506–1519.

(2) Al-Hashimi, H. M., and Walter, N. G. (2008) RNA Dynamics: It is about time. *Curr. Opin. Struct. Biol. 18*, 321–329.

(3) Jucker, F. M., Phillips, R. M., McCallum, S. A., and Pardi, A. (2003) Role of a heterogeneous free state in the formation of a specific RNA-theophylline complex. *Biochemistry 42*, 2560–2567.

(4) Latham, M. P., Zimmermann, G. R., and Pardi, A. (2009) NMR Chemical Exchange as a Probe for Ligand-Binding Kinetics in a Theophylline-Binding RNA Aptamer. *J. Am. Chem. Soc. 131*, 5052–5053.

(5) Zhang, Q., Sun, X. Y., Watt, E. D., and Al-Hashimi, H. M. (2006) Resolving the motional modes that code for RNA adaptation. *Science 311*, 653–656.

(6) Kadakkuzha, B. M., Zhao, L., and Xia, T. (2009) Conformational Distribution and Ultrafast Base Dynamics of Leadzyme. *Biochemistry 48*, 3807–3809.

(7) Hickerson, R., Majumdar, Z. K., Baucom, A., Clegg, R. M., and Noller, H. F. (2005) Measurement of internal movements within the 30 S ribosomal subunit using Forster resonance energy transfer. *J. Mol. Biol. 354*, 459–472.

(8) Crothers, D. M. (2001) RNA Conformational Dynamics. In *RNA* (Soll, D., Nishimura, S., and Moore, P. B., Eds.) pp 61−70, Elsevier Science Ltd., Oxford, U.K.

(9) Williamson, J. R. (2000) Induced fit in RNA-protein recognition. *Nat. Struct. Biol. 7*, 834–837.

(10) Leulliot, N., and Varani, G. (2001) Current topics in RNA-protein recognition: Control of specificity and biological function through induced fit and conformational capture. *Biochemistry 40*, 7947–7956.

(11) Xia, T. (2008) Taking femtosecond snapshots of RNA conformational dynamics and complexity. *Curr. Opin. Chem. Biol. 12*, 604–611.

(12) Weeks, K. M., Ampe, C., Schultz, S. C., Steitz, T. A., and Crothers, D. M. (1990) Fragments of the HIV-1 Tat Protein Specifically Bind TAR RNA. *Science 249*, 1281–1285.

(13) Churcher, M. J., Lamont, C., Hamy, F., Dingwall, C., Green, S. M., Lowe, A. D., Butler, P. J. G., Gait, M. J., and Karn, J. (1993) High-Affinity Binding of Tar RNA by the Human-Immunodeficiency-Virus Type-1 Tat Protein Requires Base-Pairs in the RNA Stem and Amino-Acid-Residues Flanking the Basic Region. *J. Mol. Biol. 230*, 90–110.

(14) Puglisi, J. D., Tan, R., Calnan, B. J., Frankel, A. D., and Williamson, J. R. (1992) Conformation of the TAR RNA-arginine complex by NMR spectroscopy. *Science 257*, 76–80.

(15) Aboul-ela, F., Karn, J., and Varani, G. (1995) The Structure of the Human Immunodeficiency Virus Type-1 TAR RNA Reveals Principles of RNA Recognition by Tat Protein. *J. Mol. Biol. 253*, 313–332.

(16) Aboul-ela, F., Karn, J., and Varani, G. (1996) Structure of HIV-1 TAR RNA in the absence of ligands reveals a novel conformation of the trinucleotide bulge. *Nucleic Acids Res. 24*, 3974–3981.

(17) Long, K. S., and Crothers, D. M. (1999) Characterization of the solution conformations of unbound and Tat peptide-bound forms of HIV-1 TAR RNA. *Biochemistry 38*, 10059–10069.

(18) Frank, A. T., Stelzer, A. C., Al-Hashimi, H. M., and Andricioaei, I. (2009) Constructing RNA dynamical ensembles by combining MD and motionally decoupled NMR RDCs: New insights into RNA dynamics and adaptive ligand recognition. *Nucleic Acids Res. 37*, 3670–3679.

(19) Zacharias, M., and Hagerman, P. J. (1995) The Bend in RNA Created by the Transactivation Response Element Bulge of Human-Immunodeficiency-Virus Is Straightened by Arginine and by Tat-Derived Peptide. *Proc. Natl. Acad. Sci. U.S.A. 92*, 6052–6056.

(20) Al-Hashimi, H. M., Gosser, Y., Gorin, A., Hu, W. D., Majumdar, A., and Patel, D. J. (2002) Concerted motions in HIV-1 TAR RNA may allow access to bound state conformations: RNA dynamics from NMR residual dipolar couplings. *J. Mol. Biol. 315*, 95–102.

(21) Pitt, S. W., Majumdar, A., Serganov, A., Patel, D. J., and Al-Hashimi, H. M. (2004) Argininamide binding arrests global motions in HIV-1 TAR RNA: Comparison with Mg^{2+}-induced conformational stabilization. *J. Mol. Biol. 338*, 7–16.

(22) Casiano-Negroni, A., Sun, X. Y., and Al-Hashimi, H. M. (2007) Probing Na^{+}-induced changes in the HIV-1 TAR conformational dynamics using NMR residual dipolar couplings: New insights into the role of counterions and electrostatic interactions in adaptive recognition. *Biochemistry 46*, 6525–6535.

(23) Zhang, Q., Stelzer, A. C., Fisher, C. K., and Al-Hashimi, H. M. (2007) Visualizing spatially correlated dynamics that directs RNA conformational transitions. *Nature 450*, 1263–1267.

(24) Nifosi, R., Reyes, C. M., and Kollman, P. A. (2000) Molecular dynamics studies of the HIV-1 TAR and its complex with argininamide. *Nucleic Acids Res. 28*, 4944–4955.

(25) Edwards, T. E., Okonogi, T. M., Robinson, B. H., and Sigurdsson, S. T. (2001) Site-specific incorporation of nitroxide spin-labels into internal sites of the TAR RNA; structure-dependent dynamics of RNA by EPR spectroscopy. *J. Am. Chem. Soc. 123*, 1527–1528.

(26) Zhang, Q., Throolin, R., Pitt, S. W., Serganov, A., and Al-Hashimi, H. M. (2003) Probing motions between equivalent RNA domains using magnetic field induced residual dipolar couplings: Accounting for correlations between motions and alignment. *J. Am. Chem. Soc. 125*, 10530–10531.

(27) Bailor, M. H., Sun, X., and Al-Hashimi, H. M. (2010) Topology links RNA secondary structure with global conformation, dynamics, and adaptation. *Science 327*, 202–206.

(28) Weeks, K. M., and Crothers, D. M. (1991) RNA Recognition by Tat-Derived Peptides: Interaction in the Major Groove? *Cell 66*, 577–588.

(29) Frankel, A. D. (1992) Peptide Models of the Tat-TAR Protein-RNA Interaction. *Protein Sci. 1*, 1539–1542.

(30) Puglisi, J. D., Chen, L., Frankel, A. D., and Williamson, J. R. (1993) Role of RNA structure in arginine recognition of TAR RNA. *Proc. Natl. Acad. Sci. U.S.A. 90*, 3680–3684.

(31) Tao, J. S., Chen, L., and Frankel, A. D. (1997) Dissection of the proposed base triple in human immunodeficiency virus TAR RNA indicates the importance of the Hoogsteen interaction. *Biochemistry 36*, 3491–3495.

(32) Calnan, B. J., Tidor, B., Biancalana, S., Hudson, D., and Frankel, A. D. (1991) Arginine-Mediated RNA Recognition: The Arginine Fork. *Science 252*, 1167–1171.

(33) Tao, J. S., and Frankel, A. D. (1992) Specific Binding of Arginine to TAR RNA. *Proc. Natl. Acad. Sci. U.S.A. 89*, 2723–2726.

(34) Tan, R. Y., and Frankel, A. D. (1992) Circular-Dichroism Studies Suggest That TAR RNA Changes Conformation Upon Specific Binding of Arginine or Guanidine. *Biochemistry 31*, 10288–10294.

(35) Ippolito, J. A., and Steitz, T. A. (1998) A 1.3-angstrom resolution crystal structure of the HIV-1 trans-activation response region RNA stem reveals a metal ion-dependent bulge conformation. *Proc. Natl. Acad. Sci. U.S.A. 95*, 9819–9824.

(36) Faber, C., Sticht, H., Schweimer, K., and Rosch, P. (2000) Structural rearrangements of HIV-1 Tat-responsive RNA upon binding of neomycin B. *J. Biol. Chem. 275*, 20660–20666.

(37) Du, Z. H., Lind, K. E., and James, T. L. (2002) Structure of TAR RNA complexed with a Tat-TAR interaction nanomolar inhibitor that was identified by computational screening. *Chem. Biol. 9*, 707–712.

(38) Al-Hashimi, H. M., Pitt, S. W., Majumdar, A., Xu, W. J., and Patel, D. J. (2003) Mg^{2+}-induced variations in the conformation and dynamics of HIV-1 TAR RNA probed using NMR residual dipolar couplings. *J. Mol. Biol. 329*, 867–873.

(39) Pitt, S. W., Zhang, Q., Patel, D. J., and Al-Hashimi, H. M. (2005) Evidence that electrostatic interactions dictate the ligand-induced arrest of RNA global flexibility. *Angew. Chem., Int. Ed. 44*, 3412–3415.

(40) Edwards, T. E., Okonogi, T. M., and Sigurdsson, S. T. (2002) Investigation of RNA-protein and RNA-metal ion interactions by electron paramagnetic resonance spectroscopy: The HIV TAR-Tat motif. *Chem. Biol. 9*, 699–706.

(41) Edwards, T. E., and Sigurdsson, S. T. (2002) Electron paramagnetic resonance dynamic signatures of TAR RNA: Small molecule complexes provide insight into RNA structure and recognition. *Biochemistry 41*, 14843–14847.

(42) Edwards, T. E., and Sigurdsson, S. T. (2003) EPR spectroscopic analysis of TAR RNA-metal ion interactions. *Biochem. Biophys. Res. Commun. 303*, 721–725.

(43) Edwards, T. E., Robinson, B. H., and Sigurdsson, S. T. (2005) Identification of amino acids that promote specific and rigid TAR RNA-tat protein complex formation. *Chem. Biol. 12*, 329–337.

(44) Bardaro, M. F., Shajani, Z., Patora-Komisarska, K., Robinson, J. A., and Varani, G. (2009) How binding of small molecule and peptide ligands to HIV-1 TAR alters the RNA motional landscape. *Nucleic Acids Res. 37*, 1529–1540.

(45) Zhang, Q., and Al-Hashimi, H. M. (2009) Domain-elongation NMR spectroscopy yields new insights into RNA dynamics and adaptive recognition. *RNA 15*, 1941–1948.

(46) Fisher, C. K., and Al-Hashimi, H. M. (2009) Approximate Reconstruction of Continuous Spatially Complex Domain Motions by Multialignment NMR Residual Dipolar Couplings. *J. Phys. Chem. B 113*, 6173–6176.

(47) Musselman, C., Zhang, Q., Al-Hashimi, H., and Andricioaei, I. (2010) Referencing Strategy for the Direct Comparision of Nuclear Magnetic Resonance and Molecular Dynamics Motional Parameters in RNA. *J. Phys. Chem. B 114*, 929–939.

(48) Olsen, G. L., Echodu, D. C., Shajani, Z., Bardaro, M. F., Varani, G., and Drobny, G. P. (2008) Solid-state deuterium NMR studies reveal μs-ns motions in the HIV-1 Transactivation response RNA recognition site. *J. Am. Chem. Soc. 130*, 2896–2897.

(49) Olsen, G. L., Michael, F., Bardaro, J., Echodu, D. C., Drobny, G. P., and Varani, G. (2010) Intermediate Rate Atomic Trajectories of RNA by Solid-State NMR Spectroscopy. *J. Am. Chem. Soc. 132*, 303–308.

(50) Ditzler, M. A., Otyepka, M., Sponer, J., and Walter, N. G. (2010) Molecular dynamics and quantum mechanics of RNA: Conformational and chemical change we can believe in. *Acc. Chem. Res. 43*, 40–47.

(51) Lee, S. W., Zhao, L., Pardi, A., and Xia, T. B. (2010) Ultrafast Dynamics Show That the Theophylline and 3-Methylxanthine Aptamers Employ a Conformational Capture Mechanism for Binding Their Ligands. *Biochemistry 49*, 2943–2951.

(52) Puglisi, J. D. (2007) The dance of domains. *Nature 450*, 1171–1172.

(53) Xia, T., Becker, H. C., Wan, C., Frankel, A., Roberts, R. W., and Zewail, A. H. (2003) The RNA-protein complex: Direct probing of the interfacial recognition dynamics and its correlation with biological functions. *Proc. Natl. Acad. Sci. U.S.A. 100*, 8119–8123.

(54) Xia, T., Wan, C. Z., Roberts, R. W., and Zewail, A. H. (2005) RNA-protein recognition: Single-residue ultrafast dynamical control of structural specificity and function. *Proc. Natl. Acad. Sci. U.S.A. 102*, 13013–13018.

(55) Zhao, L., and Xia, T. (2007) Direct Revelation of Multiple Conformations in RNA by Femtosecond Dynamics. *J. Am. Chem. Soc. 129*, 4118–4119.

(56) Liu, J. D., Zhao, L., and Xia, T. (2008) The Dynamic Structural Basis of Differential Enhancement of Conformational Stability by 5′- and 3′-Dangling Ends in RNA. *Biochemistry 47*, 5962–5975.

(57) Jain, N., Zhao, L., Liu, J. D., and Xia, T. B. (2010) Heterogeneity and Dynamics of the Ligand Recognition Mode in Purine-Sensing Riboswitches. *Biochemistry 49*, 3703–3714.

(58) Kuzmic, P. (1996) Program DYNAFIT for the analysis of enzyme kinetic data: Application to HIV proteinase. *Anal. Biochem. 237*, 260–273.

(59) Zhao, L., and Xia, T. (2009) Probing RNA Conformational Dynamics and Heterogeneity Using Femtosecond Time-resolved Fluorescence Spectroscopy. *Methods 49*, 128–135.

(60) Weeks, K. M., and Crothers, D. M. (1992) RNA-Binding Assays for Tat-Derived Peptides: Implications for Specificity. *Biochemistry 31*, 10281–10287.

(61) Bradrick, T. D., and Marino, J. P. (2004) Ligand-induced changes in 2-aminopurine fluorescence as a probe for small molecule binding to HIV-1 TAR RNA. *RNA 10*, 1459–1468.

(62) Wan, C. Z., Xia, T. B., Becker, H. C., and Zewail, A. H. (2005) Ultrafast unequilibrated charge transfer: A new channel in the quenching of fluorescent biological probes. *Chem. Phys. Lett. 412*, 158–163.

(63) Wang, S. H., Huber, P. W., Cui, M., Czarnik, A. W., and Mei, H. Y. (1998) Binding of neomycin to the TAR element of HIV-1 RNA induces dissociation of Tat protein by an allosteric mechanism. *Biochemistry 37*, 5549–5557.

(64) Fiebig, T., Wan, C., and Zewail, A. H. (2002) Femtosecond Charge Transfer Dynamics of a Modified DNA Base: 2-Aminopurine in Complexes with Nucleotides. *ChemPhysChem 3*, 781–788.

(65) Long, K. S., and Crothers, D. M. (1995) Interaction of Human-Immunodeficiency-Virus Type-1 Tat-Derived Peptides with Tar RNA. *Biochemistry 34*, 8885–8895.

(66) Wan, C., Fiebig, T., Schiemann, O., Barton, J. K., and Zewail, A. H. (2000) Femtosecond direct observation of charge transfer between bases in DNA. *Proc. Natl. Acad. Sci. U.S.A. 97*, 14052–14055.

(67) O'Neill, M. A., Becker, H. C., Wan, C., Barton, J. K., and Zewail, A. H. (2003) Ultrafast dynamics in DNA-mediated electron transfer: Base gating and the role of temperature. *Angew. Chem., Int. Ed. 42*, 5896–5900.

(68) Stelzer, A. C., Kratz, J. D., Zhang, Q., and Al-Hashimi, H. M. (2010) RNA Dynamics by Design: Biasing Ensembles Towards the Ligand-Bound State. *Angew. Chem., Int. Ed. 49*, 5731–5733.

(69) Hermann, T., and Westhof, E. (1999) Docking of cationic antibiotics to negatively charged pockets in RNA folds. *J. Med. Chem. 42*, 1250–1261.

(70) Eisenmesser, E. Z., Bosco, D. A., Akke, M., and Kern, D. (2002) Enzyme dynamics during catalysis. *Science 295*, 1520–1523.

(71) Eisenmesser, E. Z., Millet, O., Labeikovsky, W., Korzhnev, D. M., Wolf-Watz, M., Bosco, D. A., Skalicky, J. J., Kay, L. E., and Kern, D. (2005) Intrinsic dynamics of an enzyme underlies catalysis. *Nature 438*, 117–121.

(72) Gilbert, S. D., and Batey, R. T. (2006) Riboswitches: Fold and function. *Chem. Biol. 13*, 805–807.

(73) Wheeler, T. M., Sobczak, K., Lueck, J. D., Osborne, R. J., Lin, X., Dirksen, R. T., and Thornton, C. A. (2009) Reversal of RNA dominance by displacement of protein sequestered on triplet repeat RNA. *Science 325*, 336–339.

(74) Pushechnikov, A., Lee, M. M., Childs-Disney, J. L., Sobczak, K., French, J. M., Thornton, C. A., and Disney, M. D. (2009) Rational design of ligands targeting triplet repeating transcripts that cause RNA dominant disease: Application to myotonic muscular dystrophy type 1 and spinocerebellar ataxia type 3. *J. Am. Chem. Soc. 131*, 9767–9779.

(75) Velagapudi, S. P., Seedhouse, S. J., and Disney, M. D. (2010) Structure-activity relationships through sequencing (StARTS) defines optimal and suboptimal RNA motif targets for small molecules. *Angew. Chem., Int. Ed. 49*, 3816–3818.

(76) Hermann, T. (2002) Rational ligand design for RNA: The role of static structure and conformational flexibility in target recognition. *Biochimie 84*, 869–875.

(77) Parsons, J., Castaldi, M. P., Dutta, S., Dibrov, S. M., Wyles, D. L., and Hermann, T. (2009) Conformational inhibition of the hepatitis C virus internal ribosome entry site RNA. *Nat. Chem. Biol. 5*, 823–825.

(78) Lind, K. E., Du, Z. H., Fujinaga, K., Peterlin, B. M., and James, T. L. (2002) Structure-based computational database screening, in vitro assay, and NMR assessment of compounds that target TAR RNA. *Chem. Biol. 9*, 185–193.

(79) Davis, B., Afshar, M., Varani, G., Murchie, A. I. H., Karn, J., Lentzen, G., Drysdale, M., Bower, J., Potter, A. J., Starkey, I. D.,

Swarbrick, T., and Aboul-ela, F. (2004) Rational design of inhibitors of HIV-1 TAR RNA through the stabilisation of electrostatic "hot spots". *J. Mol. Biol. 336*, 343–356.

(80) Murchie, A. I. H., Davis, B., Isel, C., Afshar, M., Drysdale, M. J., Bower, J., Potter, A. J., Starkey, I. D., Swarbrick, T. M., Mirza, S., Prescott, C. D., Vaglio, P., Aboul-ela, F., and Karn, J. (2004) Structure-based drug design targeting an inactive RNA conformation: Exploiting the flexibility of HIV-1 TAR RNA. *J. Mol. Biol. 336*, 625–638.